

A Semantic-Aware and Multi-Guided Network for Infrared-Visible Image Fusion

Xiaoli Zhang*
zhangxiaoli@jlu.edu.cn
Jilin University, China

Liying Wang
liyingw23@mails.jlu.edu.cn
Jilin University, China

Libo Zhao
zhaolb20@mails.jlu.edu.cn
Jilin University, China

Xiongfei Li
lxf@jlu.edu.cn
Jilin University, China

Siwei Ma
swma@pku.edu.cn
Peking University, China

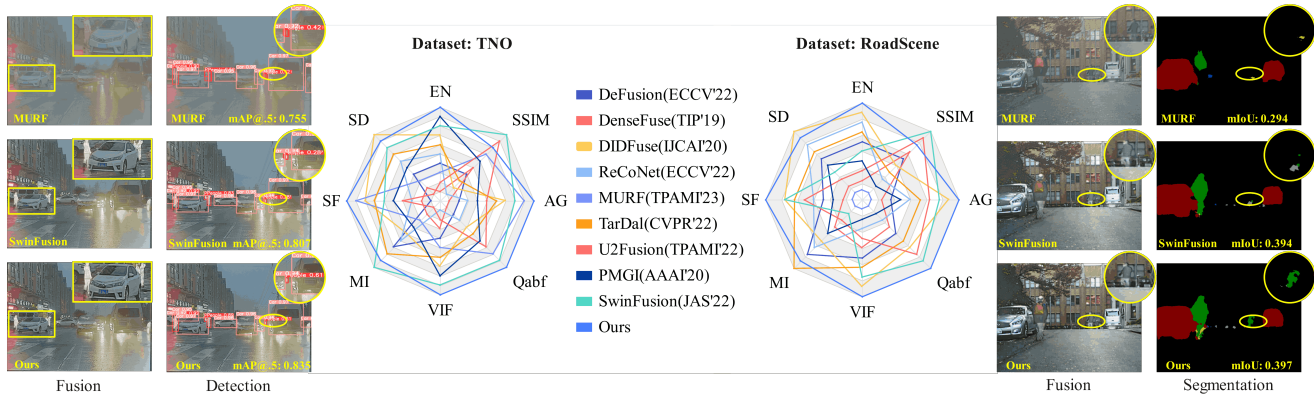


Figure 1. Fusion, detection and segmentation comparisons with state-of-art methods on TNO, RoadScene, M³FD and MFNet datasets. We show the results by radar plots and zoomed-in-patches.

Abstract

Multi-modality image fusion aims at fusing specific-modality and shared-modality information from two source images. By efficiently extracting complementary features, this paper focuses on how to model correlation-driven decomposing features and reason high-level graph nodes and edges embedding to tackle the problem of insufficient feature extraction and multi-guided feature aggregation. We propose a three branches framework with two significant components, the encoder-decoder architecture and two fusion layers. The transformer with Multi-Dconv Transposed Attention(MDTA) and Local-enhanced Feed Forward network(LeFF) is used to extract shallow features after the depthwise convolution and

is also as part of reconstruction. In the three branches encoder, Cross Attention and Invertible Block (CAI) is used to extract local features and preserve high-frequency texture details. Transformer with residual connections can capture long-range dependency and enhance shared-modality expression capability. Graph Reasoning Module(GR) is introduced to reason high-level cross-modality relations and model low-level details information as CAI's specific-modality complementary features. Experiments demonstrate that our method has obtained competitive results compared with state-of-art methods in VIF task. And we show the performances applied to MIF task and two main downstream tasks additionally, object detection and semantic segmentation.

CCS Concepts: • Computing methodologies → Computer vision..

Keywords: image fusion, feature aggregation, auto-encoder, graph neural network, invertible neural network

ACM Reference Format:

Xiaoli Zhang, Liying Wang, Libo Zhao, Xiongfei Li, and Siwei Ma. 2018. A Semantic-Aware and Multi-Guided Network for Infrared-Visible Image Fusion. In *Proceedings of Make sure to enter the correct conference title from your rights confirmation email (Conference acronym 'XX')*. ACM, New York, NY, USA, 9 pages. <https://doi.org/XXXXXX.XXXXXXX>

Permission to make digital or hard copies of all or part of this work for personal or classroom use is granted without fee provided that copies are not made or distributed for profit or commercial advantage and that copies bear this notice and the full citation on the first page. Copyrights for components of this work owned by others than the author(s) must be honored. Abstracting with credit is permitted. To copy otherwise, or republish, to post on servers or to redistribute to lists, requires prior specific permission and/or a fee. Request permissions from permissions@acm.org. Conference acronym 'XX', June 03–05, 2018, Woodstock, NY

© 2018 Copyright held by the owner/author(s). Publication rights licensed to ACM.

ACM ISBN 978-1-4503-XXXX-X/18/06
<https://doi.org/XXXXXX.XXXXXXX>

1 INTRODUCTION

Multi-modal image fusion has aroused much attention, because of the shortcomings of single modal imaging. For example, in infrared and visible fusion field, infrared imaging enables to highlight thermal targets especially in harsh environment but suffers low resolution. In addition, visible imaging can preserve abundant texture details but easily affected by the illumination conditions. Therefore, integrating two modal images effectively can researchers utilize their strengths such as visual perception and salient objects. And fused images are possible to better adapt to complex scenarios, especially serving for downstream tasks like object detection[1] and semantic segmentation[2]. Besides, image fusion has wide applications and also extends to other computer vision tasks, e.g. video surveillance[3], remote sensing[4], object tracking[5] and so on.

In recent years, deep learning methods are widely used to the image fusion field. For multi-modality images, the key issue for image fusion is to extract complementary feature from different imaging sensors and then merge them into a single image. Based on generative adversarial network(GAN), the generative-base methods[6, 7] train the generator to generate fused images and train the discriminator to force fused images similar to the source images. GANs-based methods suffer from unstable training and mode collapse, which are difficult to cope with. Recently, denoising diffusion probabilistic models(DDPM)[8] have been used in image fusion, enabling a better understanding of image generation process.

The cooperative training methods[9, 10] aim to explore relationships between image fusion and the downstream task. Some algorithms also combine differentiable neural architecture search(NAS)[11] into the training process to be suitable for specific scenario applications. Meta-learning[12, 13] is another joint training way to generate features according to designed network ability. Honestly speaking, collaborative training still has a long way to go in terms of exploring the fit between theory and practice.

The Auto-Encoder(AE) based methods[14–16] use encoding network in order to get more useful features from source images. Then favorable fusion strategies are designed to fuse features extracted from encoder architecture. Finally, the fused image is obtained by decoder's reconstruction. In view of the correlation between high and low frequency domain, correlation-driven dual-branch AE method has been proposed by[17]. The structure of encoding and decoding parts has been improved to extract deep feature, fusion strategies are also improved for better fusion performance. However, concentrating on the extraction of complementary information, exist methods can hardly fully extract features so that generated fused images always show insufficient perceptual-aware properties and poor edge-preservation. Firstly, encoder composed of powerful extracting feature

modules and decoder composed of reconstruct feature modules should be proposed to acquire desirable features from infrared and visible source images concretely. Secondly, despite of encoder's previous feature extraction, it's unavoidable to lose important feature during transmission before fusion layers to aggregate different modalities of features, especially high frequency features extracted by convolutional neural networks(CNN). In addition, as for unsupervised learning, it's necessary to design proper loss function to constraint training stage and promote fused images reasonable for human visual system(HVS) and with excellent characteristics from two modalities. In a word, we aim to propose a novel auto-encoder method to focus on the above issues, achieve better visual performance and produce task-oriented fused images.

1.1 Contributions

To solve these problems, we propose novel two-training stage encoder-decoder architecture. In the first training phase, splendid feature extraction capabilities are trained to serve for the following second training stage. Cross attention and invertible neural network(CAI) is applied to reduce information loss when transmission, at the same time enhance detail feature extracting ability. Modified residual transformer with Multi-Dconv Transposed Attention(MDTA) and Local-enhanced Feedforward Network(LeFF) is mainly used for obtaining global features with long-range dependencies. Base transformer with MDTA and LeFF is used for extracting shallow feature in encoder and as part of decoder reconstructing the target image. Graph Reasoning module is applied to model and reason high-level relations and also help extract detail feature as the balance between detail feature branch and global feature branch and extract low-level detail features simultaneously. A novel loss function aims to lead reconstruction image similar to two source images in stage I and highlight the fused images' object intensities and detail textures in training stage II. In this paper, we have four contributions as follows:

- We proposed a three branches framework with two significant components to fully extract shallow and deep features. Graph Reason Module is used in encoder to reason high-level cross-modality relations, also as the complementary features of detail features.
- The Cross Attention and Invertible neural network is proposed to extract high-frequency detail features and preserve important information efficiently when transmission. Modified Residual Transformer is applied to model long-range dependencies and obtain powerful global base feature.

- A novel loss function based on Lovasz-Softmax and Gram matrix is introduced to better utilize semantic details and intensity targets respectively to reconstruct source images. Correlation-driven decomposition loss is proposed to trade off specific-modality, shared-modality and graph-interaction features.
- Experiments show the method we proposed has satisfactory visual performance when compared with state-of-the-art methods on four datasets and in two main downstream tasks, object detection and semantic segmentation.

2 Proposed Method

2.1 Two Training Stages

Our method has two training stages and uses an encoder-decoder architecture. The encoder first extracts global features through the transformer block, and then enters three branches to extract different kinds of features; the decoder includes a transformer and multi-layer convolution operations to restore the fused features extracted from the encoder to the expected image.

Stage I – Through loss functions' constraints, the encoder-decoder architecture reconstructs both infrared and visible images, with the target of obtaining the ideal reconstructed images is as consistent as possible with the source images. As the preparation for stage II – generating fused images, training at the first stage improves encoder's ability to extract and integrate detail features, base global features and high-level reasoning relations after global features' extraction and decoder's ability to reconstruct images.

Stage II – Based on the trained encoder, multi-branch structure fully extracts intensity and semantic characteristics from two modalities. Detail features and base features after aggregations are enhanced and by two fused layers respectively, then the fused image is generated through the decoder. In the second training stage, graph interaction module's correlation coefficient is introduced to balance specific-modality information and shared-modality information, which also leads to supplement the extraction of detailed features.

2.2 Multi-guided Feature Extraction

2.2.1 Cross Attention and Feature Invertible Module. We propose cross attention module, owing to the ability of local feature extraction and aggregate the information from CNN's dual branches through interactive cross attention mechanism[18, 19] and information invertibility.

$$F_1 = \text{Attention}(Q_2, K_1, V_1) \quad (1)$$

$$F_2 = \text{Attention}(Q_1, K_2, V_2) \quad (2)$$

$$\text{Attention}(Q_2, K_1, V_1) = V_2 * \text{Softmax}(K_1, Q_2/T) \quad (3)$$

$$\text{Attention}(Q_1, K_2, V_2) = V_1 * \text{Softmax}(K_2, Q_1/T) \quad (4)$$

according to equation(3)and(4), T means temperature, a learnable scaling parameter. $(Q_1, Q_2) \in R^{HW \times C}, (K_1, K_2) \in R^{CxHW},$

$(V_1, V_2) \in R^{HW \times C}$. By applying cross attention module, we divide the number of channel to the head, which achieves two branches learning attention maps simultaneously.

Invertible neural network was firstly proposed by[20], called Non-linear Independent Component Estimation(NICE), which is designed for modeling high-dimensional densities. Then, [21] used real-valued non-volume preserving(real NVP) to improve the talent of modeling natural images. [22] introduced a generative flow using invertible 1x1 convolution. Nowadays, INNs blocks have been widely used in image or video super-resolution[23], image denoising[24] and image hiding[25, 26].

$$F_1^{i+1} = F_1^i * \exp(\psi(F_2^i)) + \psi(F_2^i) \quad (5)$$

$$F_2^{i+1} = F_2^i + \psi(F_1^i) \quad (6)$$

Inspired by[17, 26, 27], we apply the improved INN block to refine the feature extracted from the above cross attention module and further enhance CNN branch's information preserving ability and efficiently obtain semantic feature as we expect. The main structure is shown in Figure.??.

$$\text{Output}(f_1^{i+1}) = (f_1^i - \psi(f_2^i)) * \exp(-\alpha(\psi(f_2^i))) \quad (7)$$

$$\text{Output}(f_2^{i+1}) = (f_2^i - \psi(f_1^i)) * \exp(-\alpha(\psi(f_1^i))) \quad (8)$$

The i th layer designed for fusing cross-modality detail feature is shown as equation(7)and(8). Eventually, the last two layers' features are concatenated into the decoder part.

2.2.2 Base Feature Extraction Module. Using multi-channel transposed attention(MDTA), transformer implements channel-dimension self attention rather than spatial dimension. It computes cross-covariance across channels to generate an attention map to model global features with linear complexity[28]. Local-enhanced Feed Forward Network(LeFF), adding depth-wise convolution to Feed-Forward Network (FFN) aims to reduce limited capability to leverage local context[29].

$$F_{i,j} = F_{\text{transformer}}(F_{i,j-1}), j = 1, 2, \dots, L \quad (9)$$

$$F_{i,\text{out}} = F_{\text{conv}}(F_{i,L}) + F_{i,0} \quad (10)$$

where $F_{\text{transformer}}(\cdot)$ is the j -th transformer layer in the i -th residual base feature extraction block. The residual connection [30] promotes feature aggregation from different feature levels during phase of establishing long-range dependencies.

2.2.3 Graph Reasoning Module. GNNs has shown its ability concerning learning high-level relations and describing low-level details simultaneously[31]. It has been applied to image fusion field[32, 33]. This module we proposed is composed of node embedding, edge embedding, information delivery and node update, aiming at hierarchically reason about relations between two modalites and exploring useful information.

Graph Creation. We set $C = [c_1, c_2, \dots, c_n]$ and $D = [d_1, d_2, \dots, d_n]$ visible and infrared images as nodes. The directed graph $G = (V, E)$ includes nodes and edges between two

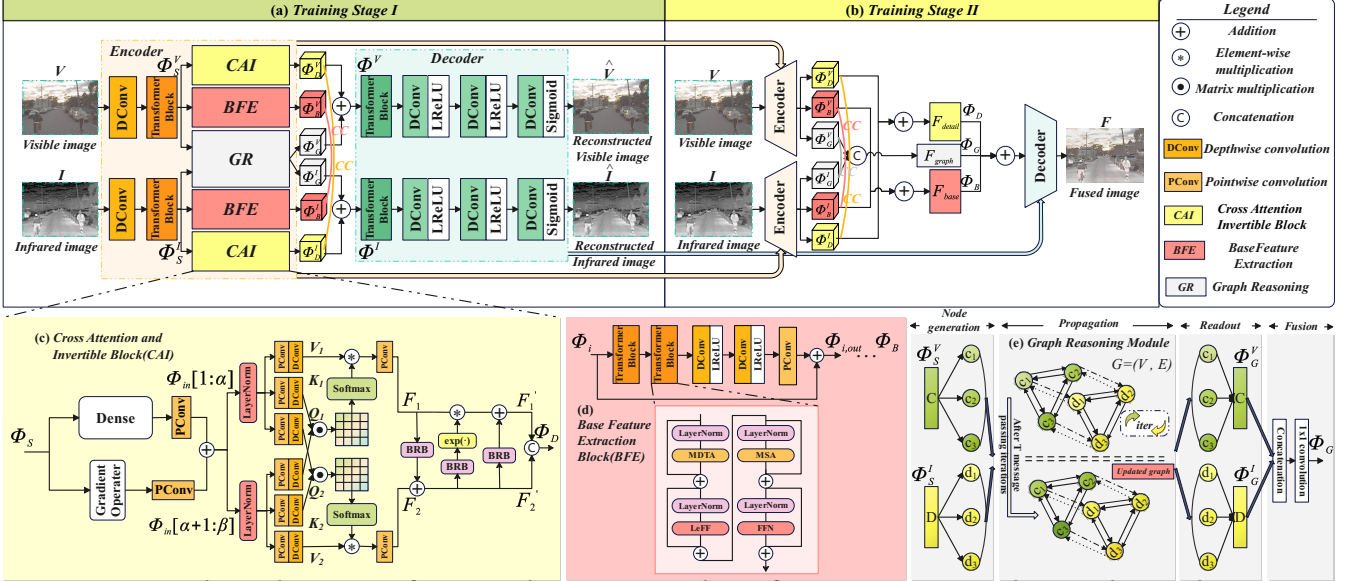


Figure 2. The architecture of proposed SMFNet. Pipeline of training stage I and II are shown above.

nodes. The inner nodes $V = V_1 \cup V_2$. When starting a graph, $c_i \leftrightarrow c_j$ and $d_i \leftrightarrow d_j$ stand for the same modality but different scales, $c_i \leftrightarrow d_i$ stands for the same scale but different modalities meanwhile.

Multi-scale Nodes Embedding. Each scale nodes have the shape $c_i^{(0)} \in R^{h \times w \times c}, d_i^{(0)} \in R^{h \times w \times c}$. For nodes generation,

$$C_i^{(0)} = R_{h \times w}(\text{Conv}(PPM(C; S_i))) \quad (11)$$

$PPM(\cdot)$ implements triple branch pooling and convolution operations.

Edges Embedding. Assume that $v_k, v_l \in V$, therefore, we obtain edges generation scheme:

$$e_{k,l} = \text{Conv}(g_{cb}(v_k; v_l)) \in R^{h \times w \times c} \quad (12)$$

$$g_{cb}(v_k; v_l) = v_l - v_k \quad (13)$$

Information delivery. After nodes and edges generation, information is transferred from current node to the other one via powerful edges. We set $m_{k,l}^{(t)}$ as message while delivering.

$$m_{k,l}^{(t)} = \sum_{k \in N(l)} M(v_k^{(t-1)}, e_{k,l}^{(t-1)}) \quad (14)$$

$$m_{k,l}^{(t)} = \sum_{k \in N(l)} \text{Sigmoid}(e_{k,l}^{(t-1)}) \cdot v_k^{(t-1)} \in R^{h \times w \times c} \quad (15)$$

Nodes Update. Next to the message delivery, GR module learn intricate cross-modality relations and nodes are updated through a GRU mechanism so that we obtain current new node as $V^{(t)}$,

$$V_l^{(t)} = \sum_{k \in N(l)} U_{GRU}(v_l^{(t-1)}, m_{k,l}^{(t-1)}) \quad (16)$$

Then, C and D can be merged separately through the convolution operation.

2.3 Loss Function

In training stage I, the total loss is shown as follows:

$$L_{total}^1 = L_{vi} + L_{ir} + \alpha_1 L_{decomp}^1 + \alpha_2 L_{grad} \quad (17)$$

where L_{vi} and L_{ir} are the reconstruction losses for visible and infrared images. L_{decomp} is feature decomposition loss and L_{grad} is spatial gradient loss. In equation(17), α_1 and α_2 are tuning parameters. Both reconstruction losses have the same L_{SSIM} and L_{grad} .

$$L_{vi} = \alpha_3 L_{SSIM}(V, \hat{V}) + L_{Semantic}(V, \hat{V}) + \beta_1 L_{grad}(V, \hat{V}) \quad (18)$$

as detailed explanation, $L_{SSIM}(V, \hat{V}) = 1 - SSIM(V, \hat{V})$ and $L_{grad}(V, \hat{V}) = |||\nabla V|, |\nabla \hat{V}||_1$. $SSIM(\cdot)$ is the structural similarity index[34]. What's more, $L_{grad}(I, \hat{I})$ and $L_{SSIM}(I, \hat{I})$ in L_{ir} can be obtained in the same way.

$$L_{ir} = \alpha_3 L_{SSIM}(I, \hat{I}) + L_{Intensity}(I, \hat{I}) + \beta_1 L_{grad}(I, \hat{I}) \quad (19)$$

Gram matrix[35] has the advantage of extracting abstract information, $Gram(\cdot)$ means Gram matrix, which promotes to preserve salient features from the infrared modality.

$$L_{Intensity}(I, \hat{I}) = ||Gram(I), Gram(\hat{I})||_2 \quad (20)$$

With regard to semantic information restriction[36], we introduce Lovasz-Softmax loss[37, 38] to calculate the differences between reconstructed image and source image for visible modality. Intersection over Union(IoU) is a classic method used for calculating whether current pixel is well predicted.

$$\Delta(\hat{y}_i, y_i^*) = 1 - \frac{|\hat{y}_i \cap y_i^*|}{|\hat{y}_i \cup y_i^*|} \quad (21)$$

$$err(\hat{y}_i, y_i^*) = \begin{cases} 1 - y_i & \text{if } y_i * \hat{y}_i == 1 \\ y_i & \text{otherwise} \end{cases} \quad (22)$$

the semantic-based Lovasz-Softmax loss[37] can be written as follows:

$$L_{semantic} = \sum err(\hat{y}_i, y_i^*) * G(\hat{y}_i, y_i^*) \quad (23)$$

As can be seen, S_i is a vector containing reconstructed image's pixels. $G(\hat{y}_i, y_i^*)$ measures the error between current state and the last state. More details can be found in paper[37].

$$G(\hat{y}_i, y_i^*) = \Delta(S_i, y^*) - \Delta(S_{i-1}, y^*) \quad (24)$$

$$S_i = \{\hat{y}_0, \hat{y}_1, \dots, \hat{y}_i\} \quad (25)$$

Based on traditional theory and correlation concept, [17] make the assumption that modality-specific information has the lower value of correlation coefficient and modality-shared information has the higher correlation value. $CC(\cdot)$ denote correlation coefficient. δ is set to 1.01, which can guarantee gradient descent and optimization.

$$L_{decomp}^1 = \frac{(CC(f_{detail}))^2}{CC(f_{base}) + \delta} \quad (26)$$

Note that high-frequency information shows more texture and details, but low-frequency information emphasis background and base feature. $f_{interact}$ aims to balance features extracted from other branches and also as the complementary for simple modality-specific features.

$$L_{decomp}^2 = \frac{(CC(f_{detail}))^2 + (CC(f_{interact}))^2}{CC(f_{base}) + \delta} \quad (27)$$

In training stage II, the total loss is:

$$L_{total}^2 = L_{intensity}^2 + \alpha_4 L_{decomp}^2 + \alpha_5 L_{grad}^2 \quad (28)$$

L_{decomp}^2 is the equation(27), $L_{intensity}$ and L_{grad} are inspired by [9], which are applied for building the restriction among fused images and source images.

$$L_{intensity}^2 = ||I_f - \max(|I_{ir}|, |I_{vi}|)||_1 \quad (29)$$

$$L_{grad}^2 = ||\nabla I_f - \max(|\nabla I_{ir}|, |\nabla I_{vi}|)||_1 \quad (30)$$

3 Experiments

3.1 Experimental Implementation

Experiment Configuration. As for the experiment part, we choose 1083 MSRS pairs as the training set and 50 Road-Scene pairs as the validation set, the testing set consists of TNO[39](25 pairs), RoadScene[40](50 pairs) and MSRS[36](36 pairs). In the training stage, all MSRS images are firstly converted to gray images and then they are cropped into 128x128 patches. There are totally 120 epochs, in fact. Training stage one has 40 epochs and the second stage has the other 80 epochs. The batch size is set to 6. As for hyperparameters in the loss function equation(17), (18) and (27), α_1 , α_2 are uniformly set to 2 and 5, α_3 , β_1 are uniformly set to 8 and 10 in training stage I. α_4 , α_5 are set to 10 and 2 in training stage II. We use Adam optimizer and initial learning rate is 1e-4 without weight decay. Experiments are executed on

the PC with two NVIDIA GeForce 4090 GPUs and pytorch framework.

Comparision Settings. There are eight evaluation metrics: Entropy(EN), standard deviation(SD), spatial frequency(SF), mutual information(MI), sum of correlations of differences(S-CD), visual information fidelity(VIF), Qabf, average gradient(AG) and structural similarity index measure(SSIM). These metrics can be found in[41] and [17]. We compare evaluation metrics with these methods: DeFusion[42], DenseFuse[14], DIDFuse[43], MURF[44], ReCoNet[45], SwinFusion[19], TarDAL[1], U2Fusion[40] and PMGI[46]. Note that we directly test fusion results on the three datasets without any fine-tuning. The larger values of the above metrics means better image quality performance.

3.2 Infrared-Visible Fusion Results

Qualitative comparison. In this section, we show qualitative results concerning TNO, RoadScene and MSRS datasets in Fig. 3. By serious observation and comparison, our method embody satisfactory visual performance compared with other state-of-the-art methods. For example, targets in dark environment can be highlighted, such as the people and cars. In addition, clear background in visible scene enables to show rich texture details. Take notice to the light, we can observe the clear shape and contour information.

Quantitative comparison. In Tab. , we list eight evaluation metrics in three testing sets for quantitative analysis. Concretely, the highest EN and AG indicates a large amount of source images' information preserved in our fused images benefiting from cross attention invertible module and reasonable complementary feature aggregation. Aware to target's edge contours is extently due to semantic loss function. Additionally, we achieve the highest values of VIF and Qabf, which mean generated fused images have excellent visual performance fit for human visual system and are also task-oriented for other computer vision tasks. Besides, the highest SF and the second-best value of MI and SSIM demonstrate good structure similarity and texture details in our results.

3.3 Infrared-visible object detection

Setup. The M^3FD dataset was firstly proposed by[1]. We use 4200 visible images and divide them into 8:1:1 as training, validation and testing set, respectively. There are totally 100 training epochs. The batch size is 8 and optimizer is SGD with initial learning rate of 1e-2. The six categories are people, car, bus, motorbike, truck and lamp. MAP@.5 is used to evaluate object detection in VIF task, especially for object detection in fused images.

Compared with SOTA methods. Table. 2 displays that SMFNet has the best detection performance, in almost all six classes, w-hich demonstrates that SMFNet can not only highlight targets difficult to detect, but also preserve fundamental texture information as for describing items themselves.

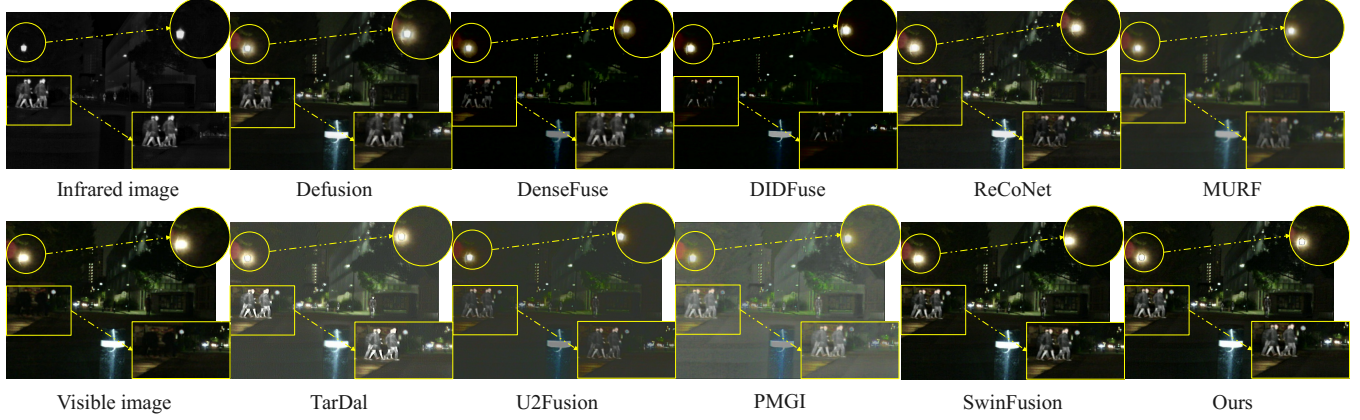
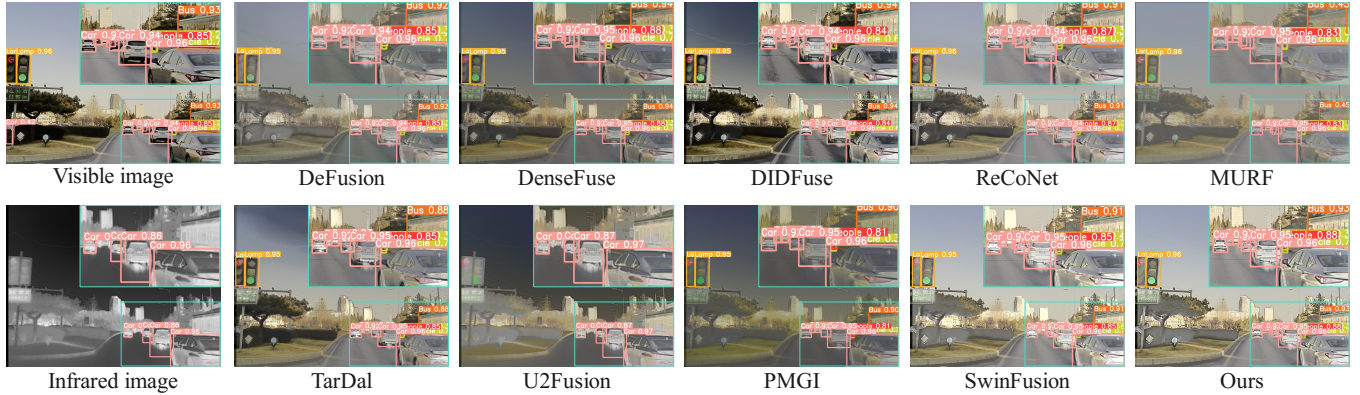


Figure 3. Qualitative fusion results on MSRS dataset.

Table 1. Quantitative experiment results of IVF task. Red indicates the best results, Blue shows the second-best values.

Method	TNO Infrared-Visible Fusion Dataset							RoadScene Infrared-Visible Fusion Dataset							MSRS Infrared-Visible Fusion Dataset									
	EN	SD	SF	MI	VIF	Qabf	AG	SSIM	EN	SD	SF	MI	VIF	Qabf	AG	SSIM	EN	SD	SF	MI	VIF	Qabf	AG	SSIM
Defusion[42]	6.5828	30.9861	6.5973	1.7573	0.5528	0.3589	3.7822	0.9401	6.8545	34.4052	7.7822	2.1668	0.5746	0.4129	4.3117	0.9011	6.3825	35.4282	8.1468	2.0686	0.7304	0.5067	3.7396	0.9154
DenseFuse[14]	6.2965	27.1425	7.0023	1.4947	0.5519	0.3394	3.7325	0.9501	6.6234	28.5042	7.4016	1.985	0.562	0.3688	3.9822	0.9377	4.7287	26.2808	6.3539	1.4026	0.4298	0.2899	2.6237	0.3792
DIDFuse[43]	6.8621	46.8716	11.7683	1.6953	0.5931	0.4033	6.0095	0.8414	7.3207	52.8861	13.6309	2.0969	0.6215	0.4855	7.3586	0.894	4.5002	29.6771	9.6158	1.4373	0.3054	0.2038	2.9108	0.2569
ReCoNet[45]	6.6775	40.4573	7.958	1.7181	0.5307	0.3728	4.7424	0.8336	7.1903	46.5624	9.753	2.1219	0.5491	0.3848	5.5852	0.8322	6.501	40.0413	9.0682	2.1484	0.6927	0.4913	4.5338	0.8299
MURF[44]	6.5402	30.7797	12.2408	1.6282	0.5566	0.4286	6.3707	0.9871	1.8689	21.6954	7.1072	1.4761	0.2033	0.1562	3.6145	0.4086	6.1556	28.5848	4.7218	1.6651	0.4269	0.1583	2.4601	0.4595
TarDal[1]	6.7795	40.6012	11.4994	1.9477	0.5677	0.4113	5.8702	0.9393	7.0848	42.7459	11.1432	2.4321	0.5826	0.4386	5.7274	0.8738	6.3476	35.4603	9.8727	1.8341	0.6728	0.4255	4.3889	0.7136
U2Fusion[40]	6.4175	26.337	8.8514	1.3468	0.5391	0.4251	5.0897	1.0214	6.7108	29.507	10.2725	1.8396	0.5599	0.4914	5.7803	0.9888	4.9532	18.869	6.7124	1.3533	0.4742	0.315	2.9513	0.6132
PMGI[46]	6.9519	35.832	8.9051	1.6512	0.6034	0.4119	5.0468	0.9781	6.7964	31.9394	7.5574	2.0768	0.5442	0.3591	4.333	0.829	5.8333	18.1081	6.0163	1.3504	0.6175	0.2731	3.0761	0.5257
SwinFusion[19]	6.8998	41.1725	11.372	2.3132	0.7572	0.5381	6.1813	1.0487	6.8274	31.7477	12.8767	1.7429	0.6093	0.584	6.8742	0.9995	6.6185	42.9849	11.0554	3.3303	1.0056	0.6693	4.9865	1.0248
Ours	7.1106	43.9525	13.6222	2.1574	0.7846	0.584	7.2613	1.0125	7.3909	51.7062	16.4399	2.3024	0.7328	0.5831	8.6128	0.9554	6.7021	42.9562	11.6976	3.1131	1.0448	0.7097	5.4765	0.9923

Figure 4. Qualitative detection results on M^3FD dataset.Table 2. Detection Quantitative results comparisons of our method with nine state-of-the-art methods on M^3FD dataset.

Method	mAP@.5						mAP@.5
	People	Car	Bus	Lamp	Motor	Truck	
DeFusion[42]	0.644	0.888	0.823	0.799	0.628	0.796	0.763
DenseFuse[14]	0.696	0.911	0.847	0.856	0.627	0.828	0.794
DIDFuse[43]	0.649	0.911	0.832	0.846	0.678	0.829	0.791
ReCoNet[45]	0.697	0.914	0.855	0.886	0.7	0.842	0.816
MURF[44]	0.641	0.872	0.806	0.809	0.645	0.759	0.755
TarDal[1]	0.647	0.878	0.82	0.779	0.639	0.844	0.768
U2Fusion[40]	0.499	0.681	0.482	0.136	0.318	0.498	0.436
PMGI[46]	0.606	0.866	0.786	0.735	0.484	0.751	0.705
SwinFusion[19]	0.69	0.919	0.85	0.868	0.683	0.83	0.807
Ours	0.723	0.925	0.862	0.903	0.738	0.856	0.835

Table 3. Segmentation Quantitative results comparisons of our method with nine state-of-the-art methods on $MFNet$ dataset.

Method	IoU							mAcc	mIoU	
	Unlabel	Car	Person	Bike	Curve	stop	Cone			
DeFusion	0.962	0.673	0.415	0.387	0.157	0.100	0.199	0.113	0.624	0.339
DenseFuse	0.961	0.658	0.390	0.480	0.154	0.118	0.298	0.267	0.610	0.376
DIDFuse	0.961	0.649	0.439	0.429	0.084	0.100	0.287	0.206	0.587	0.356
ReCoNet	0.963	0.693	0.410	0.493	0.167	0.110	0.310	0.065	0.581	0.360
MURF	0.957	0.592	0.285	0.379	0.054	0.086	0.284	0.008	0.567	0.294
TarDal	0.964	0.697	0.414	0.448	0.102	0.091	0.267	0.093	0.628	0.347
U2Fusion	0.944	0.317	0.348	0.048	0.005	0.023	0.116	0.122	0.569	0.214
PMGI	0.957	0.573	0.296	0.294	0.061	0.124	0.201	0.229	0.646	0.312
SwinFusion	0.965	0.703	0.440	0.483	0.167	0.135	0.315	0.280	0.637	0.394
ours	0.965	0.700	0.427	0.499	0.187	0.122	0.328	0.268	0.640	0.397

3.4 Infrared-visible semantic segmentation

Setup. We choose DeepLabv3+[47] as the backbone to conduct semantic segmentation. In this experiment, MFNet dataset is divided into training and test sets with nine categories(*i.e.*, back-ground, car, person, bike, curve, car stop, color clone, guardrail and bump). The model is supervised by cross entropy loss with SGD optimizer and initial learning rate of 1e-2. There are totally 300 epoches. The mean accuracy(mACC) and mean intersection-over-union(mIoU) are main evaluation metrics.

Compared with SOTA methods. The results of eight categories(unlabelled, car, person, bike, curve, car stop, color cone and bump) are shown in table 3. SMFNet has shown competitive results, especially in bike and cone. SMFNet can better integrate the edge and contour information and makes semantic segmentation more accurate.

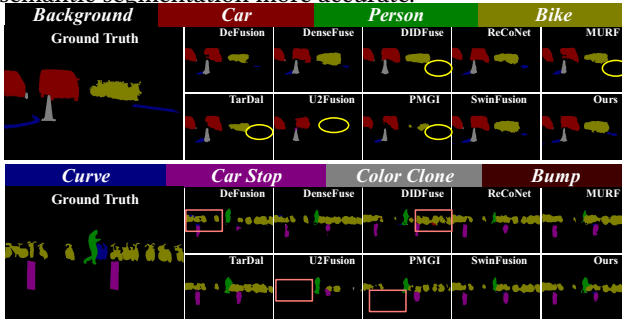


Figure 5. Visual comparisions of semantic segmentation about Fused images from the above eight fusion methods on the MFNet dataset. The proposed method can get competitive results. The yellow and pink regions show missing and error segmentation, respectively.

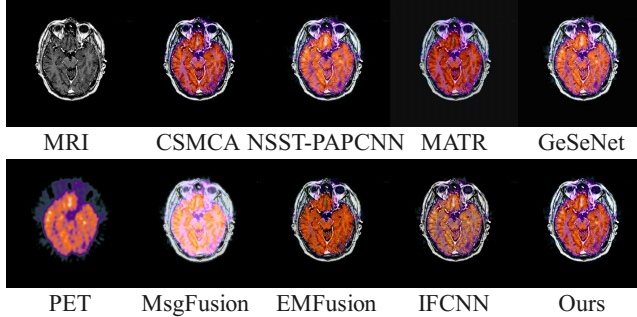


Figure 6. Fused images from the above eight fusion methods on MIF dataset.

3.5 Extension to Medical Fusion

As an extension task to validate our method's generalization, We select 270 pairs medical images on the Harvard Medical Website, including MRI-CT, MRI-PET and MRI-SPECT as training set for the MIF task. There are 20 pairs MRI-CT, 41 pairs MRI-PET and 72 pairs MRI-SPECT as testing sets.

Table 4. Extensive MRI-PET fusion experiment on Harvard Medical Dataset. Ours* represents the results after training on MIF datasets compared with other classic medical image fusion methods.

Method	MI	SF	VIF	Qabf	AG	SSIM
U2Fusion[40]	1.3879	12.2345	0.364	0.1933	3.8837	0.2086
TarDAL[1]	1.6094	18.1134	0.4268	0.3641	5.0768	0.2124
SDNet[55]	1.4763	13.2658	0.3514	0.1773	3.4486	0.2241
ReCoNet[45]	1.4408	11.1291	0.3717	0.1777	4.5917	0.2236
DeFusion[42]	1.5514	20.322	0.4439	0.4537	5.8414	1.5674
Ours	1.7284	32.6262	0.5881	0.7179	9.2834	0.3267
CSMCA[48]	1.603	33.9865	0.5604	0.6939	8.95	1.5506
NSST-PAPCNN[49]	1.6361	31.4735	0.5407	0.6594	8.6443	1.4757
MATR[50]	1.7516	25.6819	0.689	0.7202	7.3149	0.2793
GeSeNet[51]	1.6475	30.5983	0.5187	0.6844	8.8408	0.3049
MsgFusion[52]	1.6138	21.5543	0.3802	0.3814	6.0622	1.4825
EMFusion[53]	1.644	30.4133	0.559	0.6879	8.4637	1.5531
IFCNN[54]	1.5663	32.7834	0.5292	0.6874	8.9715	1.6058
Ours*	1.8031	32.3699	0.6739	0.7366	9.0584	1.6155

Because hyperparameters are set the same as VIF task, we don't need the validation set. The compared methods are CSMCA[48], NSST-PAPCNN[49], MATR[50], GeSeNet[51], MsgFusion[52], EMFu- sion[53] and IFCNN[54]. The fused medical images and evaluation metrics results are listed in Figure.?? and Table.4.

4 ABLATION STUDY

Analysis on Modules. To validate the proposed CAI's efficiency, we use basic INN block as its replacement. The performance got worse without the cross attention to enhance semantic local feature extraction. Additionally, we use stacked transformer blocks as capturing low-frequency information branch in encoder. Results demonstrate that residual connections combined with CNNs bring better long-range expression abilities. Last but not least, we exchange two fusion layers indicating their proper positions for the fusion stage.

Features Decomposition and Aggregation. In this part, we discuss proposed intensity and semantic losses in training stage I and correlation-driven GNN loss proposed in training stage II. Gram matrix bring salient targets and proposed Lovasz-Softmax loss maintain much texture details. GNN Loss leading in the second stage further enhances cross-modality interaction and balance between high-frequency and low-frequency information.

Two Training Stages. To validate the importance of two training stages, we directly train encoder, decoder and fusion layers together. The results are unsatisfactory. In fact, pre-trained encoder and decoder show more powerful feature extraction abilities and promote training in the second stage to generate better performance on qualitative and quantitative results.

Table 5. Ablation experiment results in the test set of RoadScene. Red indicates the best results and blue means the second-best results.

Configurations	EN	SD	VIF	SSIM
two-stage both cc_G	7.3765	51.4596	0.7248	0.9333
w/o two stage training	7.365	50.4629	0.6906	0.9237
w/o intensity and semantic loss	7.3579	50.7396	0.7297	0.9401
w/o residual transformer	7.3592	50.4884	0.7056	0.9291
CAI->INN block	7.3257	49.5447	0.7139	0.9417
w/o GNN	7.3692	50.9436	0.7027	0.9102
INN<->transformer	7.3584	50.8266	0.7247	0.9482
Ours	7.3909	51.7062	0.7328	0.9554

5 CONCLUSION

In this paper, we proposed a correlation-driven multi-feature aggregation framework for infrared and visible image fusion, including three branches and two significant components. The Cross-Attention Invertible neural network module is proposed to extract detail features and preserve high frequency information. Modified Residual Transformer block extracts long-range dependencies as shared-modality feature. Graph Reasonable Module is used to model high-level cross-modality relations and extract low-level details as detail complementary information in the encoder. A novel loss function based on Lovasz- Softmax and Gram matrix is proposed as restriction concerning two training stages. Experiments demonstrate the fusion effect of our SMFNet and the accuracy of downstream pattern recognition tasks can be improved.

Acknowledgments

To Robert, for the bagels and explaining CMYK and color spaces.

References

- [1] Jinyuan Liu, Xin Fan, Zhanbo Huang, Guanyao Wu, Risheng Liu, Wei Zhong, and Zhongxuan Luo. Target-aware dual adversarial learning and a multi-scenario multi-modality benchmark to fuse infrared and visible for object detection. In *Proceedings of the IEEE/CVF Conference on Computer Vision and Pattern Recognition*, pages 5802–5811, 2022.
- [2] Jinyuan Liu, Zhu Liu, Guanyao Wu, Long Ma, Risheng Liu, Wei Zhong, Zhongxuan Luo, and Xin Fan. Multi-interactive feature learning and a full-time multi-modality benchmark for image fusion and segmentation. In *Proceedings of the IEEE/CVF international conference on computer vision*, pages 8115–8124, 2023.
- [3] Nirmala Paramanandham and Kishore Rajendiran. Infrared and visible image fusion using discrete cosine transform and swarm intelligence for surveillance applications. *Infrared Physics & Technology*, 88:13–22, 2018.
- [4] Wele Gedara Chaminda Bandara and Vishal M Patel. Hypertransformer: A textural and spectral feature fusion transformer for pan-sharpening. In *Proceedings of the IEEE/CVF conference on computer vision and pattern recognition*, pages 1767–1777, 2022.
- [5] Yabin Zhu, Chenglong Li, Bin Luo, Jin Tang, and Xiao Wang. Dense feature aggregation and pruning for rgbt tracking. In *Proceedings of the 27th ACM International Conference on Multimedia*, pages 465–472, 2019.
- [6] Jiayi Ma, Han Xu, Junjun Jiang, Xiaoguang Mei, and Xiao-Ping Zhang. Ddcgan: A dual-discriminator conditional generative adversarial network for multi-resolution image fusion. *IEEE Transactions on Image Processing*, 29:4980–4995, 2020.
- [7] Jiayi Ma, Wei Yu, Pengwei Liang, Chang Li, and Junjun Jiang. Fusiongan: A generative adversarial network for infrared and visible image fusion. *Information fusion*, 48:11–26, 2019.
- [8] Zixiang Zhao, Haowen Bai, Yuanzhi Zhu, Jiangshe Zhang, Shuang Xu, Yulun Zhang, Kai Zhang, Deyu Meng, Radu Timofte, and Luc Van Gool. Ddfm: denoising diffusion model for multi-modality image fusion. In *Proceedings of the IEEE/CVF International Conference on Computer Vision*, pages 8082–8093, 2023.
- [9] Linfeng Tang, Jiteng Yuan, and Jiayi Ma. Image fusion in the loop of high-level vision tasks: A semantic-aware real-time infrared and visible image fusion network. *Information Fusion*, 82:28–42, 2022.
- [10] Zhu Liu, Jinyuan Liu, Benzhuang Zhang, Long Ma, Xin Fan, and Risheng Liu. Paif: Perception-aware infrared-visible image fusion for attack-tolerant semantic segmentation. In *Proceedings of the 31st ACM International Conference on Multimedia*, pages 3706–3714, 2023.
- [11] Hanxiao Liu, Karen Simonyan, and Yiming Yang. Darts: Differentiable architecture search. *arXiv preprint arXiv:1806.09055*, 2018.
- [12] Wenda Zhao, Shigeng Xie, Fan Zhao, You He, and Huchuan Lu. Meta-fusion: Infrared and visible image fusion via meta-feature embedding from object detection. In *Proceedings of the IEEE/CVF Conference on Computer Vision and Pattern Recognition*, pages 13955–13965, 2023.
- [13] Haowen Bai, Zixiang Zhao, Jiangshe Zhang, Yichen Wu, Lilun Deng, Yukun Cui, Shuang Xu, and Baisong Jiang. Refusion: Learning image fusion from reconstruction with learnable loss via meta-learning. *arXiv preprint arXiv:2312.07943*, 2023.
- [14] Hui Li and Xiao-Jun Wu. Densefuse: A fusion approach to infrared and visible images. *IEEE Transactions on Image Processing*, 28(5):2614–2623, 2018.
- [15] Hui Li, Xiao-Jun Wu, and Tariq Durrani. Nestfuse: An infrared and visible image fusion architecture based on nest connection and spatial/channel attention models. *IEEE Transactions on Instrumentation and Measurement*, 69(12):9645–9656, 2020.
- [16] Jinyuan Liu, Yuhui Wu, Zhanbo Huang, Risheng Liu, and Xin Fan. Smoa: Searching a modality-oriented architecture for infrared and visible image fusion. *IEEE Signal Processing Letters*, 28:1818–1822, 2021.
- [17] Zixiang Zhao, Haowen Bai, Jiangshe Zhang, Yulun Zhang, Shuang Xu, Zudi Lin, Radu Timofte, and Luc Van Gool. Cddfuse: Correlation-driven dual-branch feature decomposition for multi-modality image fusion. In *Proceedings of the IEEE/CVF Conference on Computer Vision and Pattern Recognition*, pages 5906–5916, 2023.
- [18] Yuanshen Guan, Ruikang Xu, Mingde Yao, Lizhi Wang, and Zhiwei Xiong. Mutual-guided dynamic network for image fusion. In *Proceedings of the 31st ACM International Conference on Multimedia*, pages 1779–1788, 2023.
- [19] Jiayi Ma, Linfeng Tang, Fan Fan, Jun Huang, Xiaoguang Mei, and Yong Ma. Swinfusion: Cross-domain long-range learning for general image fusion via swin transformer. *IEEE/CAA Journal of Automatica Sinica*, 9(7):1200–1217, 2022.
- [20] Laurent Dinh, David Krueger, and Yoshua Bengio. Nice: Non-linear independent components estimation. *arXiv preprint arXiv:1410.8516*, 2014.
- [21] Laurent Dinh, Jascha Sohl-Dickstein, and Samy Bengio. Density estimation using real nvp. *arXiv preprint arXiv:1605.08803*, 2016.
- [22] Durk P Kingma and Prafulla Dhariwal. Glow: Generative flow with invertible 1x1 convolutions. *Advances in neural information processing systems*, 31, 2018.
- [23] Man Zhou, Keyu Yan, Jie Huang, Zihe Yang, Xueyang Fu, and Feng Zhao. Mutual information-driven pan-sharpening. In *Proceedings of the IEEE/CVF Conference on Computer Vision and Pattern Recognition*,

pages 1798–1808, 2022.

[24] Yang Liu, Zhenyu Qin, Saeed Anwar, Pan Ji, Dongwoo Kim, Sabrina Caldwell, and Tom Gedeon. Invertible denoising network: A light solution for real noise removal. In *Proceedings of the IEEE/CVF conference on computer vision and pattern recognition*, pages 13365–13374, 2021.

[25] Junpeng Jing, Xin Deng, Mai Xu, Jianyi Wang, and Zhenyu Guan. Hinet: deep image hiding by invertible network. In *Proceedings of the IEEE/CVF international conference on computer vision*, pages 4733–4742, 2021.

[26] Zhenyu Guan, Junpeng Jing, Xin Deng, Mai Xu, Lai Jiang, Zhou Zhang, and Yipeng Li. Deepmih: Deep invertible network for multiple image hiding. *IEEE Transactions on Pattern Analysis and Machine Intelligence*, 45(1):372–390, 2022.

[27] Man Zhou, Jie Huang, Keyu Yan, Danfeng Hong, Xiuping Jia, Jocelyn Chanussot, and Chongyi Li. A general spatial-frequency learning framework for multimodal image fusion. *IEEE Transactions on Pattern Analysis and Machine Intelligence*, 2024.

[28] Syed Waqas Zamir, Aditya Arora, Salman Khan, Munawar Hayat, Fahad Shahbaz Khan, and Ming-Hsuan Yang. Restormer: Efficient transformer for high-resolution image restoration. In *Proceedings of the IEEE/CVF conference on computer vision and pattern recognition*, pages 5728–5739, 2022.

[29] Zhendong Wang, Xiaodong Cun, Jianmin Bao, Wengang Zhou, Jianzhuang Liu, and Houqiang Li. Uformer: A general u-shaped transformer for image restoration. In *Proceedings of the IEEE/CVF conference on computer vision and pattern recognition*, pages 17683–17693, 2022.

[30] Jingyun Liang, Jie Zhang Cao, Guolei Sun, Kai Zhang, Luc Van Gool, and Radu Timofte. Swinir: Image restoration using swin transformer. In *Proceedings of the IEEE/CVF international conference on computer vision*, pages 1833–1844, 2021.

[31] Ao Luo, Xin Li, Fan Yang, Zhicheng Jiao, Hong Cheng, and Siwei Lyu. Cascade graph neural networks for rgb-d salient object detection. In *Computer Vision–ECCV 2020: 16th European Conference, Glasgow, UK, August 23–28, 2020, Proceedings, Part XII 16*, pages 346–364. Springer, 2020.

[32] Zhaoliang Chen, Lele Fu, Jie Yao, Wenzhong Guo, Claudia Plant, and Shiping Wang. Learnable graph convolutional network and feature fusion for multi-view learning. *Information Fusion*, 95:109–119, 2023.

[33] Jiawei Li, Jiansheng Chen, Jinyuan Liu, and Huijin Ma. Learning a graph neural network with cross modality interaction for image fusion. In *Proceedings of the 31st ACM International Conference on Multimedia*, pages 4471–4479, 2023.

[34] Zhou Wang, Alan C Bovik, Hamid R Sheikh, and Eero P Simoncelli. Image quality assessment: from error visibility to structural similarity. *IEEE transactions on image processing*, 13(4):600–612, 2004.

[35] Hui Li, Tianyang Xu, Xiao-Jun Wu, Jiwen Lu, and Josef Kittler. Lrrnet: A novel representation learning guided fusion network for infrared and visible images. *IEEE transactions on pattern analysis and machine intelligence*, 2023.

[36] Linfeng Tang, Jiteng Yuan, Hao Zhang, Xingyu Jiang, and Jiayi Ma. Piafusion: A progressive infrared and visible image fusion network based on illumination aware. *Information Fusion*, 83:79–92, 2022.

[37] Maxim Berman, Amal Rannen Triki, and Matthew B Blaschko. The lovász-softmax loss: A tractable surrogate for the optimization of the intersection-over-union measure in neural networks. In *Proceedings of the IEEE conference on computer vision and pattern recognition*, pages 4413–4421, 2018.

[38] Linfeng Tang, Yuxin Deng, Yong Ma, Jun Huang, and Jiayi Ma. Superfusion: A versatile image registration and fusion network with semantic awareness. *IEEE/CAA Journal of Automatica Sinica*, 9(12):2121–2137, 2022.

[39] Alexander Toet and Maarten A Hogervorst. Progress in color night vision. *Optical Engineering*, 51(1):010901–010901, 2012.

[40] Han Xu, Jiayi Ma, Junjun Jiang, Xiaojie Guo, and Haibin Ling. U2fusion: A unified unsupervised image fusion network. *IEEE Transactions on Pattern Analysis and Machine Intelligence*, 44(1):502–518, 2020.

[41] Jiayi Ma, Yong Ma, and Chang Li. Infrared and visible image fusion methods and applications: A survey. *Information fusion*, 45:153–178, 2019.

[42] Pengwei Liang, Junjun Jiang, Xianming Liu, and Jiayi Ma. Fusion from decomposition: A self-supervised decomposition approach for image fusion. In *European Conference on Computer Vision*, pages 719–735. Springer, 2022.

[43] Zixiang Zhao, Shuang Xu, Chunxia Zhang, Junmin Liu, Pengfei Li, and Jiangshe Zhang. Didfuse: Deep image decomposition for infrared and visible image fusion. *arXiv preprint arXiv:2003.09210*, 2020.

[44] Han Xu, Jiteng Yuan, and Jiayi Ma. Murf: Mutually reinforcing multi-modal image registration and fusion. *IEEE Transactions on Pattern Analysis and Machine Intelligence*, 2023.

[45] Zhanbo Huang, Jinyuan Liu, Xin Fan, Risheng Liu, Wei Zhong, and Zhongxuan Luo. Reconet: Recurrent correction network for fast and efficient multi-modality image fusion. In *European Conference on Computer Vision*, pages 539–555. Springer, 2022.

[46] Hao Zhang, Han Xu, Yang Xiao, Xiaojie Guo, and Jiayi Ma. Rethinking the image fusion: A fast unified image fusion network based on proportional maintenance of gradient and intensity. In *Proceedings of the AAAI conference on artificial intelligence*, volume 34, pages 12797–12804, 2020.

[47] Liang-Chieh Chen, Yukun Zhu, George Papandreou, Florian Schroff, and Hartwig Adam. Encoder-decoder with atrous separable convolution for semantic image segmentation. In *Proceedings of the European conference on computer vision (ECCV)*, pages 801–818, 2018.

[48] Yu Liu, Xun Chen, Rabab K Ward, and Z Jane Wang. Medical image fusion via convolutional sparsity based morphological component analysis. *IEEE Signal Processing Letters*, 26(3):485–489, 2019.

[49] Ming Yin, Xiaoning Liu, Yu Liu, and Xun Chen. Medical image fusion with parameter-adaptive pulse coupled neural network in nonsubsampled shearlet transform domain. *IEEE Transactions on Instrumentation and Measurement*, 68(1):49–64, 2018.

[50] Wei Tang, Fazhi He, Yu Liu, and Yansong Duan. Matr: Multimodal medical image fusion via multiscale adaptive transformer. *IEEE Transactions on Image Processing*, 31:5134–5149, 2022.

[51] Jiawei Li, Jinyuan Liu, Shihua Zhou, Qiang Zhang, and Nikola K Kasabov. Gesenet: A general semantic-guided network with couple mask ensemble for medical image fusion. *IEEE Transactions on Neural Networks and Learning Systems*, 2023.

[52] Jinyu Wen, Feiwei Qin, Jiao Du, Meie Fang, Xinhua Wei, CL Philip Chen, and Ping Li. Msgfusion: Medical semantic guided two-branch network for multimodal brain image fusion. *IEEE Transactions on Multimedia*, 2023.

[53] Han Xu and Jiayi Ma. Emfusion: An unsupervised enhanced medical image fusion network. *Information Fusion*, 76:177–186, 2021.

[54] Yu Zhang, Yu Liu, Peng Sun, Han Yan, Xiaolin Zhao, and Li Zhang. Ifcnn: A general image fusion framework based on convolutional neural network. *Information Fusion*, 54:99–118, 2020.

[55] Hao Zhang and Jiayi Ma. Sdnet: A versatile squeeze-and-decomposition network for real-time image fusion. *International Journal of Computer Vision*, 129(10):2761–2785, 2021.